JOURNAL OF MATERIALS SCIENCE 21 (1986) 3002–3014

Tetragonal → twinned hexagonal crystal phase transformation in polybutene-1

K. W. CHAU, Y. C. YANG, P. H. GEIL
Polymer Group, Department of Metallurgy and Mining Engineering, University of Illinois, Urbana, Illinois 61801, USA

The spontaneous transformation of the metastable (Form II) tetragonal crystals into the stable twinned hexagonal (Form I) crystals in polybutene-1 was studied using several techniques. The mechanical properties of the heat moulded material undergo significant changes in the process and the crystalline melting point increases from 112 to 128° C. Results from an Avrami analysis suggest the nucleation of the stable crystalline phase occurs shortly after crystallization from the melt and the subsequent growth of the nuclei follows a rod-like geometry. Transmission electron microscopy of melt-grown thin films shows that nucleation occurs at random positions within a spherulite and growth propagates along the radially oriented fibrillar crystals. As a result of multiple nucleation, each tetragonal crystal generates several twinned hexagonal crystallites with different crystallographic orientations. Besides exhibiting multiple nucleation within each individual tetragonal crystal, solution-grown single crystals also reveal twisting of the crystal lattice about the *c*-axis. The information obtained shows that residual stresses present in the material do not appear essential for the nucleation of the stable phase. Current concepts of the transformation mechanism are examined.

1. Introduction

It was discovered by Natta and co-workers [1–7] that on crystallizing from the melt, isotactic polybutene-1 (PB-1) first assumes a crystalline structure which is unstable and gradually transforms into another crystalline form on ageing. They chose to name the unstable form "Form II" and the stable form "Form I". The unit cell of Form II crystals has been described as tetragonal with the polymer chains arranged in an 11/3 helical conformation [1, 8, 9]. The unit cell of Form I crystals has been described as hexagonal (or rhombohedral) and the chains assume a 3/1 helical conformation [6]. Form II is thus also referred to as the tetragonal form while Form I is referred to as the twinned hexagonal form to distinguish it from the crystallographically similar untwinned hexagonal form (Form I′) which is obtained from solution [10, 11] or from the melt under high pressure [12].

The Form II → Form I phase transformation significantly alters the properties of the material. The crystalline melting point increases from 120 to 136° C and the material becomes increasingly turbid, more rigid and exhibits higher strength [13]. Since PB-1 parts are manufactured by heat moulding, their properties are affected by the transformation. A thorough understanding of the molecular mechanism of the transformation is highly desirable in connection with applications of the polymer. The physics of the transformation itself is also sufficiently interesting that it warrants a careful study.

A substantial amount of work has been done in attempts to characterize the nature of the transformation. The process is greatly accelerated by applied stress or high pressure. In particular, it has been stated that the transformation is essentially complete after a few seconds at 100 atm [6, 12]. Weynant *et al.* [14] studied the effects of transformation during deformation by means of optical microscopy (OM), differential scanning calorimetry (DSC) and X-ray diffraction (XRD) techniques. The unstable tetragonal crystals were found to transform into the stable twinned hexagonal form during plastic deformation. Turner-Jones [8] pointed out that the distance measured parallel to the chain axis per monomer unit is 0.187 nm in the 11/3 helix and 0.217 nm in the 3/1 helix. She suggested that since the 11/3 helix is less extended than the 3/1 helix, the tetragonal → twinned hexagonal transformation is assisted by tension.

Boor and Mitchell [13] examined the effects of the transformation by means of infrared spectroscopy, density gradient column and dilatometric contraction measurements. Luongo and Salovey [15] discovered from their infrared spectroscopic study that the rate of the phase transformation depends on the thickness of the compression moulded film, decreasing with increasing thickness from 0.002 to 0.008 in. Information concerning the molecular mechanism of transformation was obtained by several authors [16, 17] who independently carried out Avrami type of analyses. They arrived at the conclusion that the nucleation of the stable phase is instantaneous in time.

Of direct interest is a recent electron microscopy study of the phase transformation in oriented thin films and solution-grown tetragonal single crystals by Gohil *et al.* [18]. By means of dark-field diffraction contrast technique, they were able to directly observe

0022–2461/86 $03.00 + .12

the effects of the transformation. They reported the following:

1. In oriented thin films, the lateral dimensions of a lamellar crystal before and after transformation are nearly identical as can be concluded from ($h\,k\,0$) dark-field micrographs from both of these phases.
2. While the metastable tetragonal lamellae have a high degree of crystal perfection, the transformed lamellae are full of crystal defects.
3. Except for the c-axis orientation, there exists no firm lattice relationship between untransformed and transformed crystals.
4. Transformation is suppressed at temperatures below the glass transition temperature ($-10°$ C). It is, however, spontaneous at temperatures ranging from 60 to $-150°$ C, the temperature range studied, if the samples are given a slight strain (approximately 20%).
5. Monolayered tetragonal single crystals grown from a dilute solution in xylene–n-butanol mixture do not transform either when kept in the solvent or on carbon coated microscope grids for a period of more than a year. Based on these observations, they concluded that nucleation of the stable phase is the rate-determining step in the transformation process. A stable phase nucleus is thought to be created by either external applied stress or thermal stresses which develop in irregularly stacked lamellar arrangements. Stresses exerted by taut tie molecules are also believed to enhance the growth rate by providing sites for nucleation of the stable phase.

The purpose of this paper is to examine the mechanism of the tetragonal → twinned hexagonal crystal phase transformation in unoriented polybutene-1 at the molecular level, its effects on the properties of the material, and to assess current concepts of the transformation process.

2. Experimental details

2.1. Materials

Two PB-1 samples manufactured by the Shell Chemical Company, PB-H (M_n = 74000, M_w = 730000) and PB-L (M_n = 35000, M_w = 350000), were studied. They were supplied in the form of pellets.

2.2. Sample preparation

Films used in this study were crystallized from the melt. Films for DSC and X-ray diffraction studies were prepared by placing PB-1 pellets in a mould consisting of a 4 cm × 3 cm rectangular window cut out of a piece of 1 mm thick brass plate sandwiched between two pieces of aluminium foil. They were melted at 160° C for 4 min, pressed for another 4 min at a pressure of 1000 psi (7 MPa) in a Carver Press equipped with heating plates, and quenched in 20° C water. PB-1 films with a thickness of 1 mm were obtained. They were examined after being aged at room temperature for various periods of time. Care was exercised in removal of the aluminium foil and subsequent handling of the films to prevent flexure of the films since rapid transformation occurs with any deformation.

Films of varying degrees of thickness to be used for Fourier transform infrared spectroscopy (FTIR) studies were prepared in a similar manner except that the polybutylene pellets were melted at 180° C for 8 min, pressed for another 8 min at a pressure of 10000 psi (70 MPa) and quenched in air at 20° C. The thinnest films (~ 5 μm thick) to be studied with FTIR were first obtained by casting a 4% (by weight) PB-1 solution in carbon tetrachloride on clean glass slides. They were subsequently removed and melted on potassium bromide plates at 180° C and quenched in air at 20° C.

Thin films (~ 100 nm thick) for TEM were obtained by initial solution casting. A 1% (by weight) PB-1 solution in carbon tetrachloride was obtained by dissolving PB-1 pellets in carbon tetrachloride heated to 70° C. A few drops of this solution were spread on a clean glass slide and the solvent was allowed to evaporate in air at room temperature. The films were floated off on water, placed on 200 mesh electron microscope copper grids with carbon substrates, and melted in nitrogen atmosphere in an oven at 160° C for 3 min before being removed and allowed to cool in air to room temperature. Such samples were examined after being aged for different periods of time at room temperature. Some were studied without further treatment while others were shadowed with carbon/platinum at a 30° angle just prior to examination.

Thick films (~ 1 mm thick) whose surface morphology was to be studied by TEM were prepared by directly melting the PB-1 pellets on a glass slide placed in a nitrogen-filled oven at 160° C for 6 min and cooling them in air to room temperature. Carbon/platinum free surface replicas of the same areas of these samples were repeatedly prepared at different lengths of time after crystallization.

Single crystals were grown from a dilute solution in amyl acetate. A 0.01% (by weight) solution was prepared by dissolving the appropriate amount of two-day old compression moulded PB-H film (~ 0.05 mm thick) in a measured amount of amyl acetate which had been preheated to 120° C by placing it in an oven for 2 h. After dissolution, as indicated by clearing, which was completed in less than 20 min with stirring, the resulting solution was immediately removed from the oven and allowed to crystallize at room temperature. The first trace of crystals, which rendered the solution turbid, appeared about one hour after the solution had been cooled at room temperature. The suspension was kept at room temperature for another 2 h to ensure complete crystallization. A fine medicine dropper was used to deposit a few drops of the crystal suspension on a carbon substrate previously mounted on an electron microscope grid. The amyl acetate was allowed to evaporate at room temperature. The composition of the crystals prepared by this method varies considerably. Usually 0 to 30% of the crystals obtained are tetragonal crystals; the rest are of the orthorhombic (Form III) modification.

2.3. Differential scanning calorimetry (DSC)

DSC studies were made using a DuPont 1090 thermal analyser equipped with a 910 differential scanning

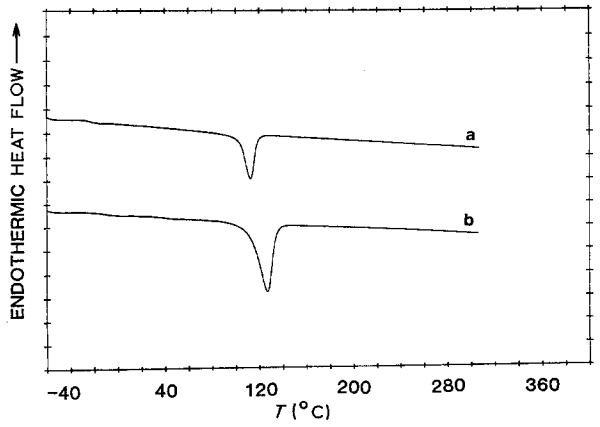

Figure 1 DSC spectra of PB-L samples. Curve (a) is the spectrum of a sample which had been left at room temperature for 1 h after quenching from the melt. Curve (b) is the spectrum of a sample which had been aged for 70 days after quenching to room temperature. Sample size was 5.8 mg in each case, ordinate scale is 2 mW per division.

calorimeter and a 1091 disc memory. The heating rate was 20° C min^{-1}. Sample size was 3 to 6 mg. Data analysis was carried out with computer software provided by DuPont Instruments Inc.

2.4. Fourier transform infrared spectroscopy (FTIR)

Infrared spectra were recorded with a Nicolet 170 SX (formerly 7199 A) Fourier transform infrared spectrometery using a resolution of 4 cm^{-1} with a total of 100 scans.

2.5. X-ray diffraction

Wide-angle X-ray diffraction scans of compression moulded films were recorded with a Philips-Norelco Type 42271/0 diffractometer as a function of ageing time using Cu$K\alpha$ radiation in the reflection mode.

2.6. Transmission electron microscopy (TEM)

A Jeol JEM 100C transmission microscope was used with examination being carried out at 100 kV. Surface morphology was studied using C/Pt free surface replicas and C/Pt shadowed thin films. Electron diffraction and dark-field electron microscopy were done using thin films and single crystals which had not been shadowed.

3. Results and discussion

3.1. Differential scanning calorimetry

Fig. 1 shows the DSC spectra of PB-L samples. Curve (a) is the spectrum of a freshly melt-crystallized sample while curve (b) is that of a sample aged 70 days at room temperature. The glass transition at −23° C is more conspicuous in the fresh sample than in the aged one. The fresh sample has a crystalline melting transition at 112° C implying that its crystalline content consists only of tetragonal crystals. The aged sample shows a crystalline melting transition at 127° C, indicating that transformation into the twinned hexagonal phase has occurred during ageing. PB-H exhibits a similar behaviour except that its corresponding crystalline melting temperatures are 116 and 128° C respectively for the fresh and aged forms – presumably a result of its higher molecular weight.

3.2. Infrared transform infrared spectroscopy

The crystalline forms (I and II) of PB produce significantly different infrared spectra from 1500 to 450 cm^{-1}. Fig. 2 shows IR spectra (1400 to 1500 cm^{-1}) of melt-crystallized PB films (~ 1.5 mm thick) aged for various time at room temperature. The bottom curve is the spectrum of a fresh sample, which represents the unstable Form II. The top curve is the spectrum of a sample aged for 1 year and represents the stable Form I. Curve 2 is from a sample aged for

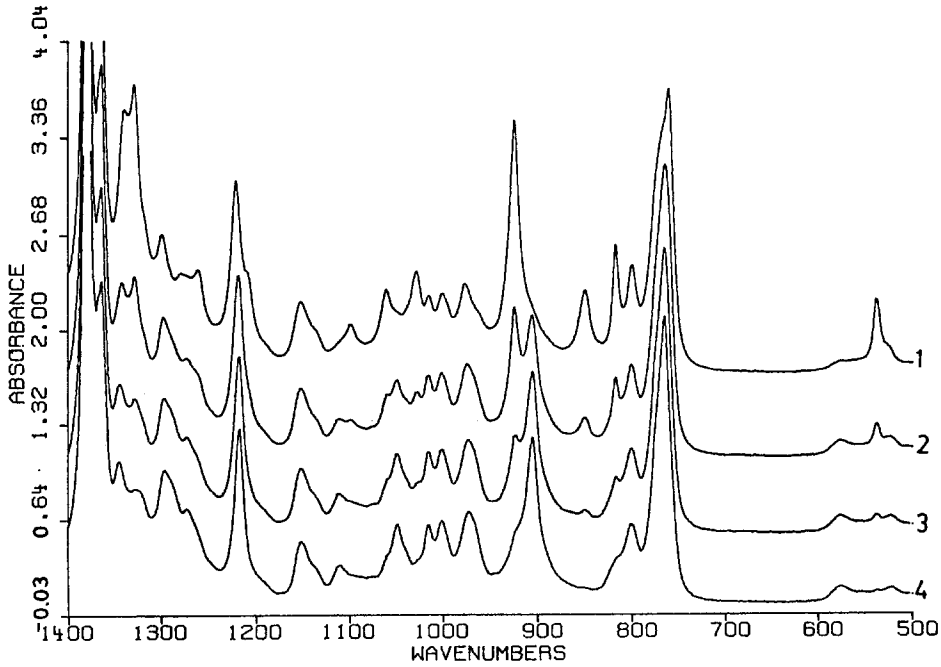

Figure 2 IR spectra of PB-1, curve 1 = aged for 1 year, curve 2 = aged for 10 h, curve 3 = aged for 2 h, curve 4 = aged for 15 min.

TABLE I Infrared absorption frequencies in PB-1

Crystal type	Frequencies						
Form I	1463.8	1463.8	1380.5	1364.6	1339.9	1328.6*	1298.6
Form II	1462.5	–	1380.2	–	1344.8	1327.0	1296.2
Form I	1278.6	–	1260.4*	1220.8*	1152.0	–	1098.5
Form II		1272.7	–	1217.2	1151.6	1111.2	–
Form I	1060.1	–	1027.9*	1014.5	1000.0	975.8	923.6*
Form II		1048.9	–	1051.1	1001.1	972.5	–
Form I		848.8*	816.1	798.8	760.1	574.2*	536.9*
Form II	904.7*	–	–	799.8	765.0	575.3	536.6
Form I	524.8*	483.2					
Form II	522.0	–					

10 h and curve 3 is from a sample aged for 2 h. A number of differences in the intensities and frequencies are noted. Table I summarizes the frequencies of the absorption peaks of Form I and Form II. The bands marked with asterisks are those discussed previously by Luongo and Salovey [15]; they reported only intensity and profile differences. By using FTIR we are able to easily observe differences in the frequencies between the crystalline forms as small as $\pm 0.1\,cm^{-1}$.

Expanded regions of Fig. 2 are shown in Figs 3 to 5. The curves are labelled in the same manner as those in Fig. 2. Two kinds of bands are noted. The "characteristic bands" are inherent to either Form I (e.g. $923.6\,cm^{-1}$) or Form II (e.g. $904.7\,cm^{-1}$). The intensities of the Form I characteristic bands increase while those of the Form II decrease upon II → I transformation. Transformation, however, has no effect on the frequencies of these bands. Some characteristic bands of Form I appear as shoulders in the spectra of the fresh samples. A small degree of transformation occurred as a result of the external stress applied to peel the PB-1 films from the aluminium foil. The other kind of bands appears only as differences of frequency between Form I and Form II: for instance, $760.1\,cm^{-1}/765.0\,cm^{-1}$. The shift in frequency from Form II to Form I occurs during ageing. These bands may result from changes of the valence co-ordinates or simply from the combination of two characteristic bands which cannot be resolved by the resolution we used. As indicated by the $904.7\,cm^{-1}$ band there is still some Form II left after ageing for 1 year.

The strong absorbance bands in the region of $1400\,cm^{-1}$ can only be characterized using thin samples. Fig. 6 is the spectra of $\sim 5\,\mu m$ thick samples which were prepared by casting from a 4% PB-1/CCl_4 solution and subsequently melted on KBr plates.

By observing the rate of transformation in films of varying thickness, we discovered that the rate of II → I transformation decreases with decreasing thickness. It is to be emphasized that this is only true for

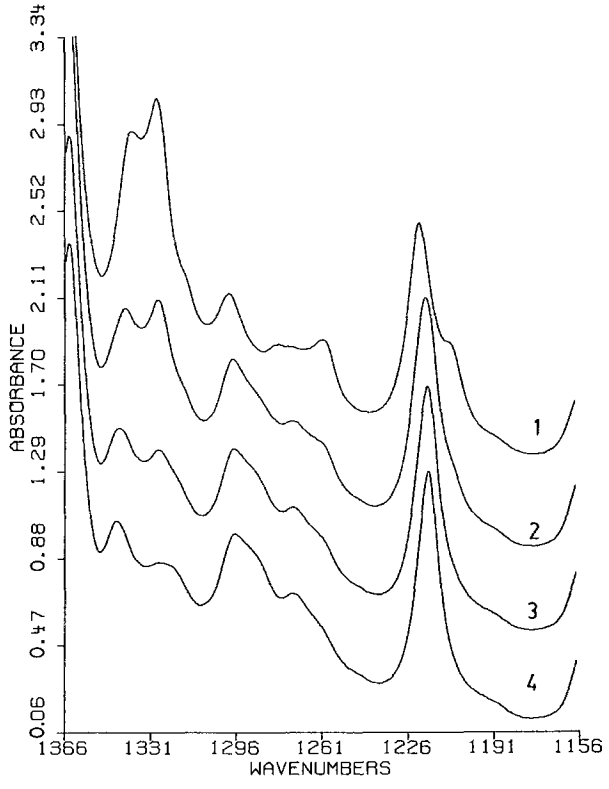

Figure 3 IR spectra of PB-1, curve 1 = aged for 1 year, curve 2 = aged for 10 h, curve 3 = aged for 2 h, curve 4 = aged for 15 min.

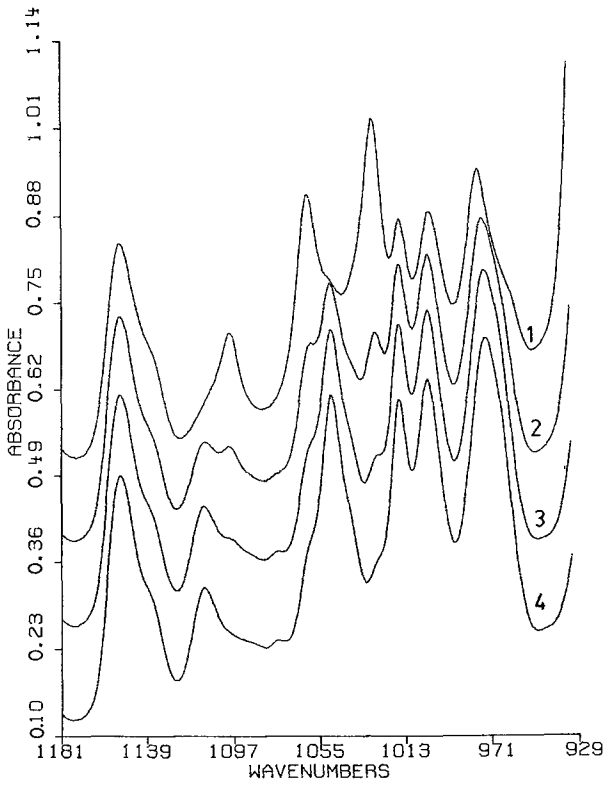

Figure 4 IR spectra of PB-1, curve 1 = aged for 1 year, curve 2 = aged for 10 h, curve 3 = aged for 2 h, curve 4 = aged for 15 min.

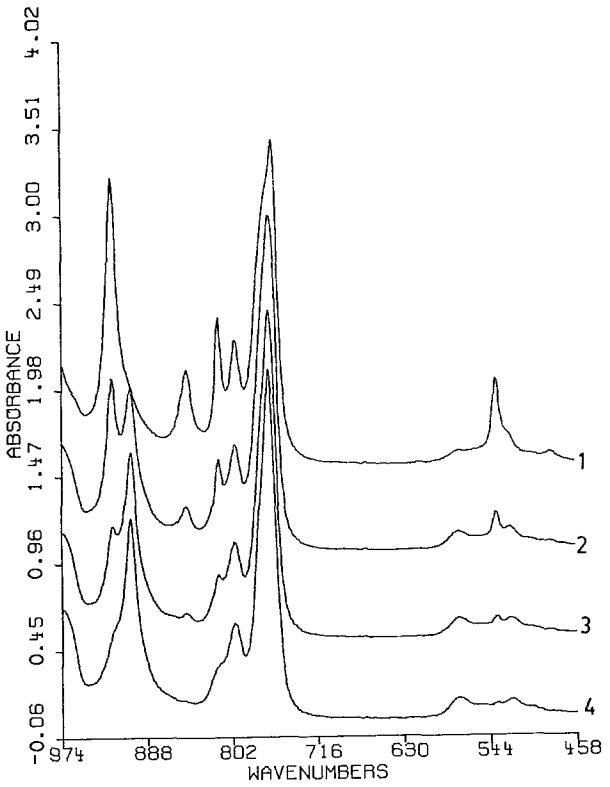

Figure 5 IR spectra of PB-1, curve 1 = aged for 1 year, curve 2 = aged for 10 h, curve 3 = aged for 2 h, curve 4 = aged for 15 min.

samples not subjected to external stress. Samples which have been subjected to external stress, such as those which have been peeled off from the moulding substrate, show a reverse relationship, i.e. the thinner the film, the faster the conversion rate, as has been reported by other authors [15, 19].

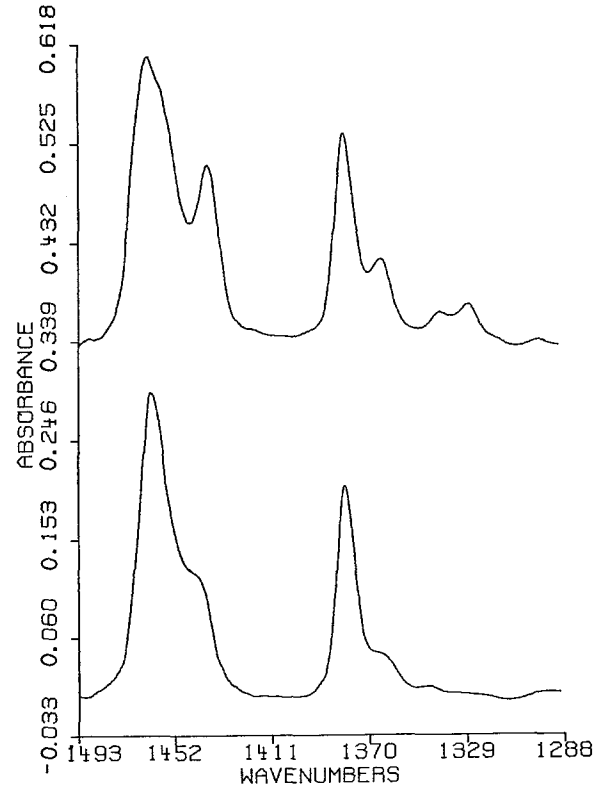

Figure 6 IR spectra of PB-1 melt-crystallized on a KBr plate, upper curve = aged for 120 days, bottom curve = aged for 15 min.

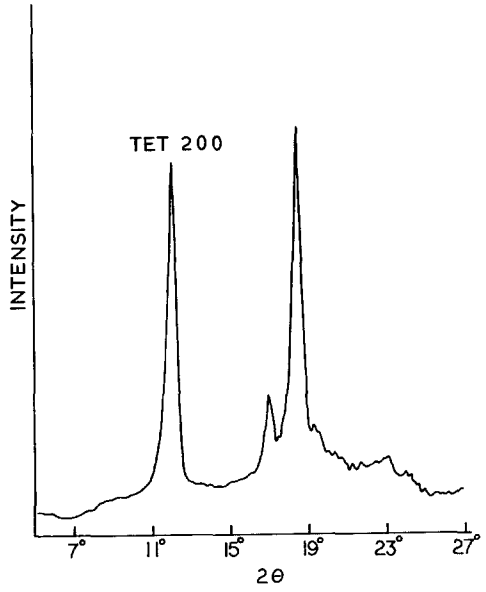

Figure 7 X-ray diffraction pattern of a PB-L film. Taken 1 h after quenching from the melt.

3.3. X-ray diffraction

Wide angle X-ray diffraction scans of a freshly crystallized PB-L sample and of the same sample after 90 days are shown in Figs 7 and 8. PB-H exhibits the same behaviour except that it transforms at a lower rate. The decrease in intensity of the tetragonal form reflections appears to cease after a period of about 1 month. It is noted that DSC scans indicate the absence of tetragonal form crystals in aged samples similar to that used to obtain the scan in Fig. 8. The rate of transformation was obtained by measuring the total area under the tetragonal 200 diffraction peak (at $2\theta \simeq 12°$) in X-ray diffractometer scans of the same sample taken as a function of time. The amount of amorphous scattering intensity was estimated from the diffracted intensity in the vicinity of $2\theta \simeq 12°$ after 3 months when the amount of unstable

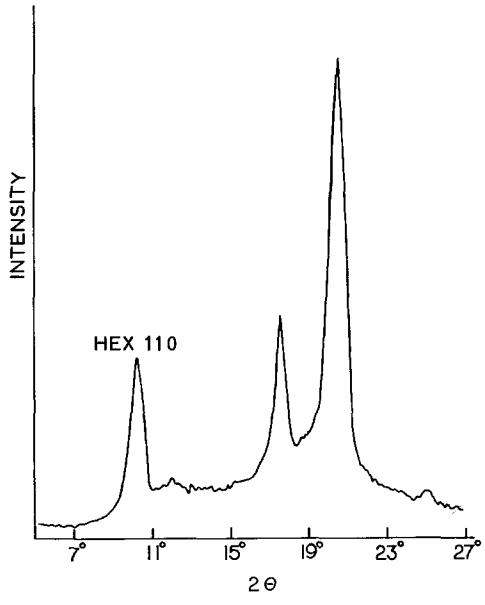

Figure 8 X-ray diffraction pattern of the same sample used to obtain the pattern in Fig. 7 after the sample had been aged for 90 days at room temperature after quenching.

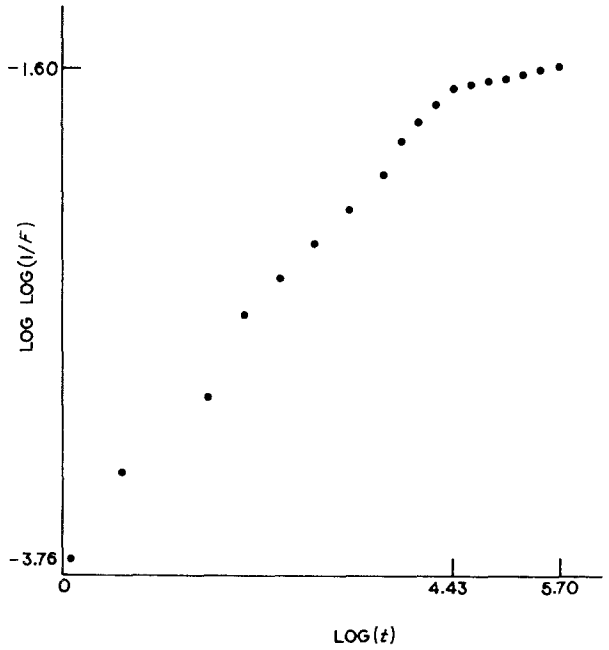

Figure 9 A plot of the negative of the natural logarithm of the fraction of tetragonal crystals remaining in a PB-L sample against ageing time t.

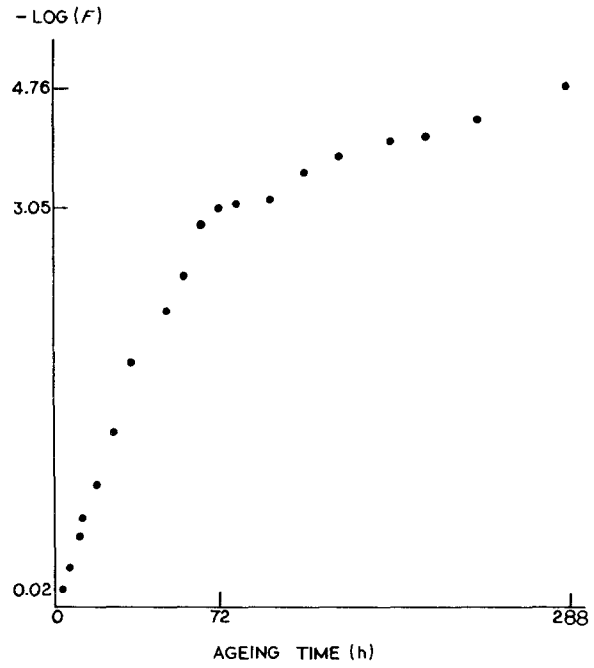

Figure 10 An Avrami plot of the phase transformation in PB-L. The ageing time t is measured in hours.

tetragonal crystals had decreased to an equilibrium value. This amorphous scattering intensity was subtracted from the total intensity of the tetragonal 200 diffraction peak in each of the previous measurements. Corrections for sample thickness were not needed since the same sample was used. It is noted that the crystallinity increases gradually during ageing at room temperature and thus this method will somewhat underestimate the initial amount of tetragonal form. The disappearance of tetragonal crystals obeys an exponential law and therefore follows a first order reaction mechanism. The fraction of tetragonal crystals remaining in a sample, F, fits the function $\exp(-rt)$, where t is the ageing time and r is the rate constant which can be obtained from the slope of the logarithmic plot shown in Fig. 9. Regression and curve-fitting of the data were carried out with a statistical analysis program [20] on the University of Illinois Plato computer system. For each PB-1 sample, the logarithmic plot shows a change in slope at 70 to 80 h. The effect is believed similar to that of secondary crystallization during initial crystallization. The rate constants for the two samples are listed in Table II.

An Avrami type of analysis [21, 22] usually used to study crystallization, can be used to analyse the transformation mechanism. The Avrami equation which related $X(t)$, the amount of transformed crystals at time t, to $X(\infty)$, the amount of transformed crystals at infinite ageing time, is given by

$$X(t) = X(\infty)[1 - \exp(zt^n)] \quad (1)$$

where z is the rate factor. The Avrami coefficient, n, whose value is related to the form of nucleation and growth of the stable phase, is obtained from the slope of a plot of log log $[1/F(t)]$ against log t (Fig. 10). Here $F(t) = [X(\infty) - X(t)]/X(\infty)$ is the fraction of crystals remaining untransformed at time t. The Avrami coefficients for the two PB-1 samples are listed in Table III.

The initial values listed are similar but somewhat smaller than those reported by Oda *et al.* [17], the latter being for another commercial polybutene-1 (Petrotex A-250′ – 53). An Avrami coefficient of 1 implies instantaneous nucleation and a one-dimensional growth geometry of the stable phase. This suggests that the nuclei form almost simultaneously and the growth of the stable phase is rod-like.

3.4. Transmission electron microscopy

Melt-crystallized PB-1 films of the different thicknesses studied are composed of spherulites which typically measure from 10 to 80 μm in diameter. Representative spherulitic surfaces from a thick film are shown in Fig. 11a. A typical micrograph of the surface of the thin films is shown in Fig. 12. In Fig. 11a the spherulite nuclei are presumably below the surface, the central sheaf not being seen. No difference is seen between PB-H and PB-L. Free surface replicas of the

TABLE II

Sample	Rate constant r for $t < 70$ h	Rate constant r for $t > 70$ h
PB-H $M_n = 74000$	0.21 h^{-1}	0.008 h^{-1}
PB-L $M_n = 35000$	0.44 h^{-1}	0.006 h^{-1}

TABLE III

Sample	Avrami coefficient for $t < 72$ h	Avrami coefficient for $t > 72$ h
PB-H	1.05	0.60
PB-L	1.14	0.25

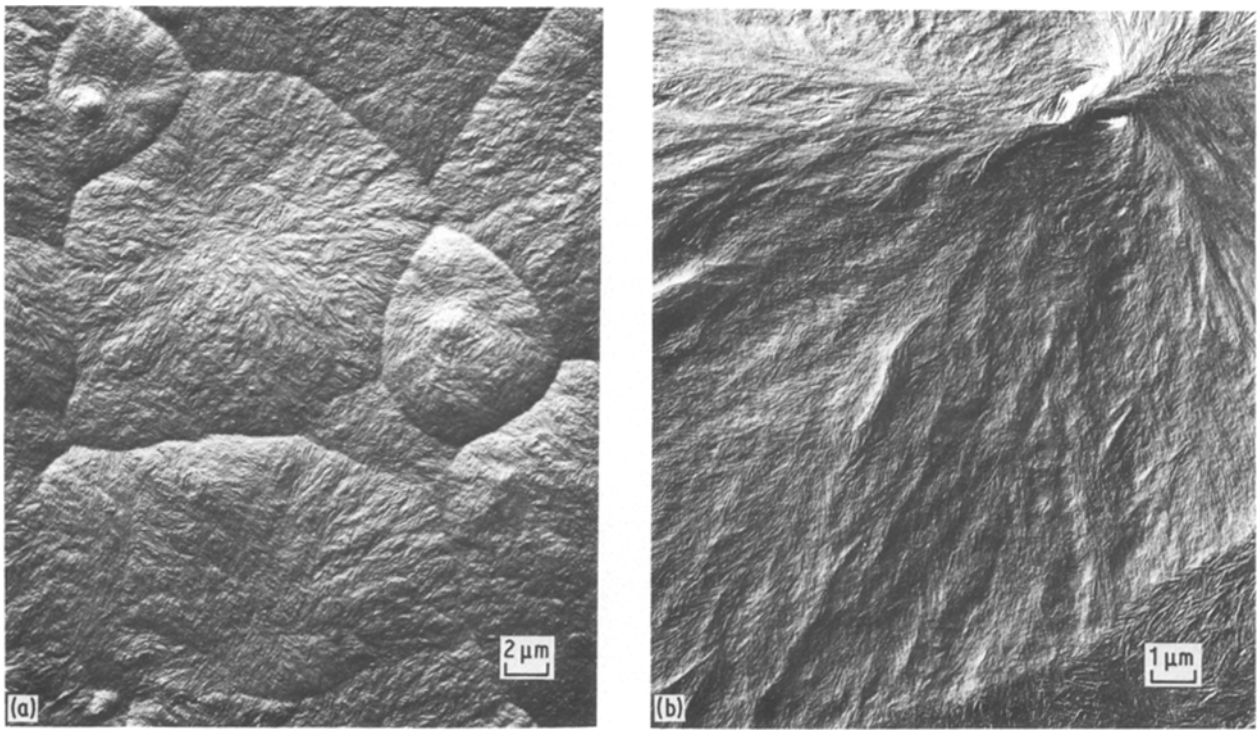

Figure 11 Free surface replicas of melt-crystallized PB-L thick films. (a) Typical replica, (b) a region revealing lamellar crystals lying nearly parallel to the sample surface.

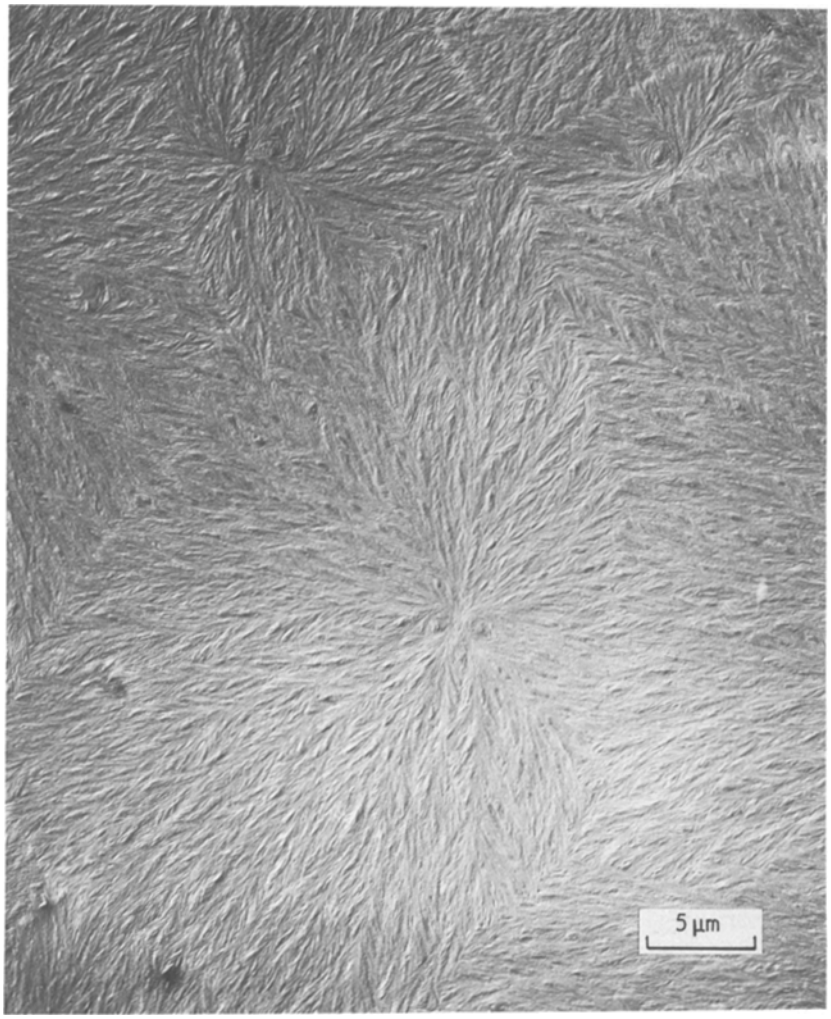

Figure 12 Micrograph showing the typical surface morphology of a melt-crystallized PB-L thin film.

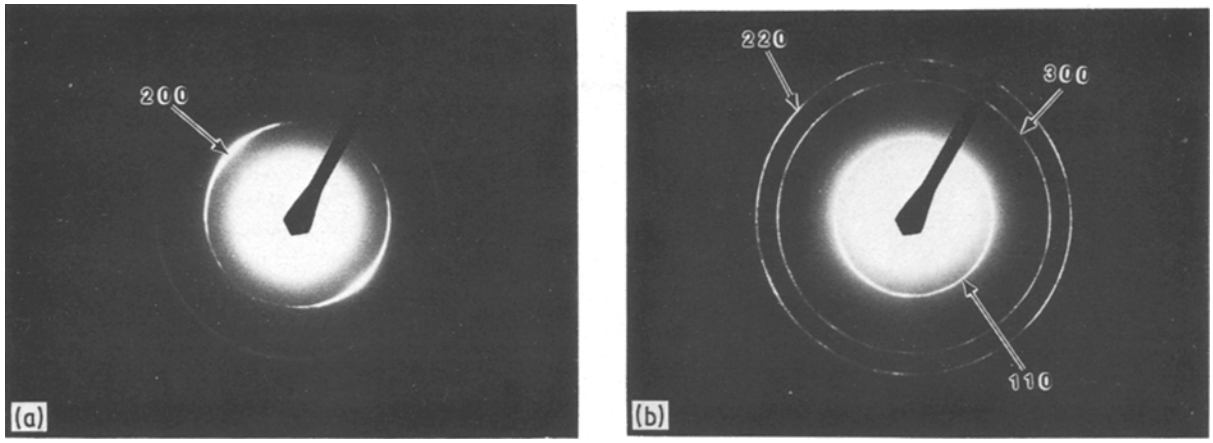

Figure 13 Typical electron diffraction patterns of the two types of crystals found in melt-crystallized PB-L thin films. (a) The tetragonal form, (b) the twinned hexagonal form.

same area of a sample prepared at various ageing times do not show any change in morphology. The phase transformation does not alter the surface morphology which is presumably determined at the moment of crystallization. Over most of the surface the crystals appear to be approximately 30 nm thick and the order of 1.5 μm long, suggesting that the crystals are fibrillar or ribbon-like in shape. In a few areas, however, as can be seen in Fig. 11b, lamellar crystals nearly parallel to the surface are present. In contrast to many other polymers, however, one cannot find any evidence of a large lateral size to the lamellae, even in slowly crystallized samples.

The two crystal forms present in the thin films are readily identified by their characteristic electron diffraction patterns. As expected, the unstable tetragonal form is the species found exclusively in fresh films. With time, the stable twinned hexagonal form appears. Normally, for both PB-H and PB-L, the first trace of twinned hexagonal crystals does not appear in the thin films until two days after crystallization and a trace of the tetragonal crystals remains even after a period of 6 months. Typical electron diffraction patterns of the two types of crystals found in PB-L thin films are shown in Fig. 13. Similar electron diffraction patterns were observed in PB-H thin films.

In typical dark-field micrographs of freshly crystallized thin films of PB-H and PB-L (Fig. 14a), the most obvious structures are the bright lines of approximately 50 nm width and up to 1.2 μm long. These tetragonal crystals are oriented in the spherulite with their length in the radial direction. Closer inspection and longer exposure (Fig. 15b) reveal irregular grey areas predominantly in areas in which the bright lines are absent. The results suggest that in these thin films, as in the thick ones in Fig. 11, most of the crystals are oriented with their width direction perpendicular to the surface; it is these that appear as bright lines in the dark-field micrographs because of their substantial thickness in the beam direction. The grey areas, on the other hand, are due to crystals lying essentially parallel to the film surface, the low intensity being due to their thinness (< 30 nm crystal thickness) in the beam direction. The small lateral size and irregularity of their outline can be due to either/or both, an actual small lateral size and curvature of the crystals out of diffracting position. It is noted that in the thin films and on the surface of the thick films, most of the crystals are oriented perpendicular to the surface such that only their lateral edge is seen. The reason for this is not known. The results suggest the tetragonal crystals are lamellae of relatively small lateral size, approaching a ribbon or lath-like shape.

Typical dark-field micrographs of aged thin films are shown in Figs 15a and b. The individual twinned hexagonal crystals are of comparable thickness to the tetragonal crystals in Fig. 14 but measure less than 0.3 μm in length. The micrographs in Figs 14 and 15 were taken under identical microscope settings (same beam size, apertures and accelerating voltage). A comparison of crystal sizes in fresh and aged samples strongly suggests that in the transformation process, each tetragonal fibril gives rise to several twinned hexagonal crystallites generally with different crystallographic orientations. Electron diffraction patterns taken from similar areas of the spherulites with the same beam size also show higher local crystalline orientation in a fresh spherulite than in an aged spherulite. Fig. 13 represents the typical situation. No evidence is seen of individual grey areas in micrographs of aged films; presumably they have also decreased in size and, possibly, merged into a general background.

Further information concerning the mechanism of the transformation can be obtained from examining areas in which the process has occurred only partially. Fig. 16 shows a typical micrograph taken from such an areas using the tetragonal 2 0 0 and hexagonal 1 1 0 diffractions. Besides showing tetragonal (long) and twinned hexagonal (short) crystals, it also reveals, in several places, individual crystallites which lie in rows. Two examples of such rows are indicated by arrows. Each row of small crystals is believed to have originated from a single tetragonal fibril. The extinct (dark) positions along each row are now occupied by crystals which are not in diffracting position. It is noted that the long tetragonal crystals and the short twinned hexagonal crystals are intermixed. This indicates the phase transformation does not sweep through a spherulite but is nucleated at random. The

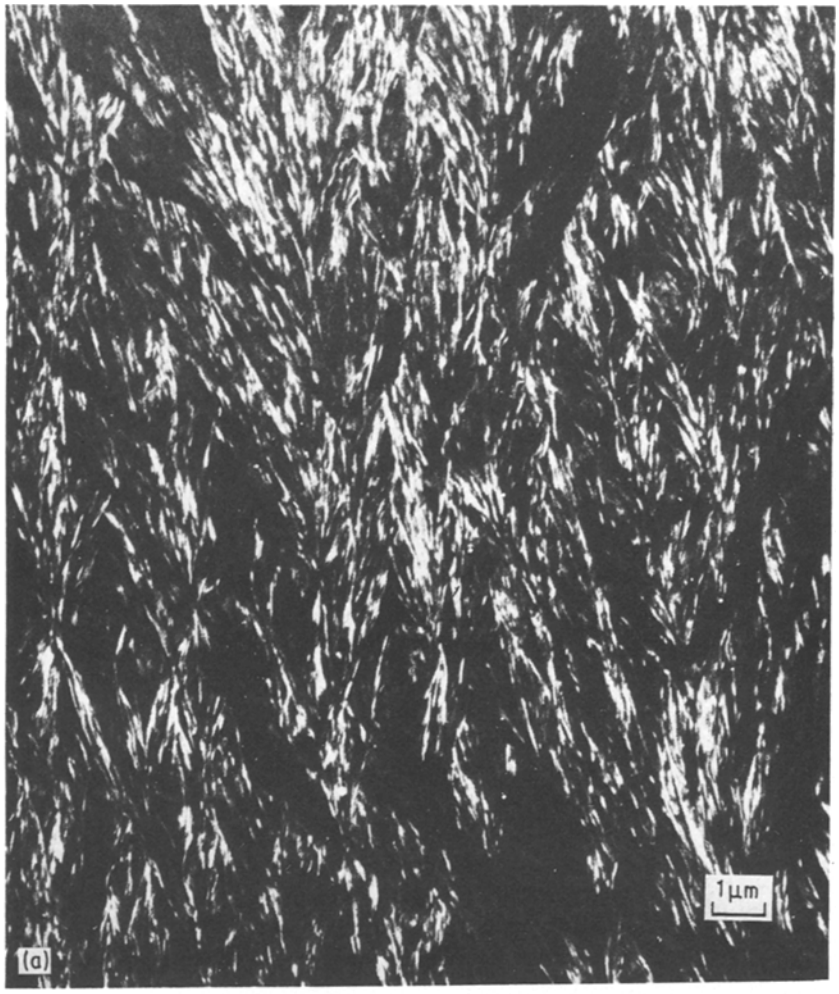

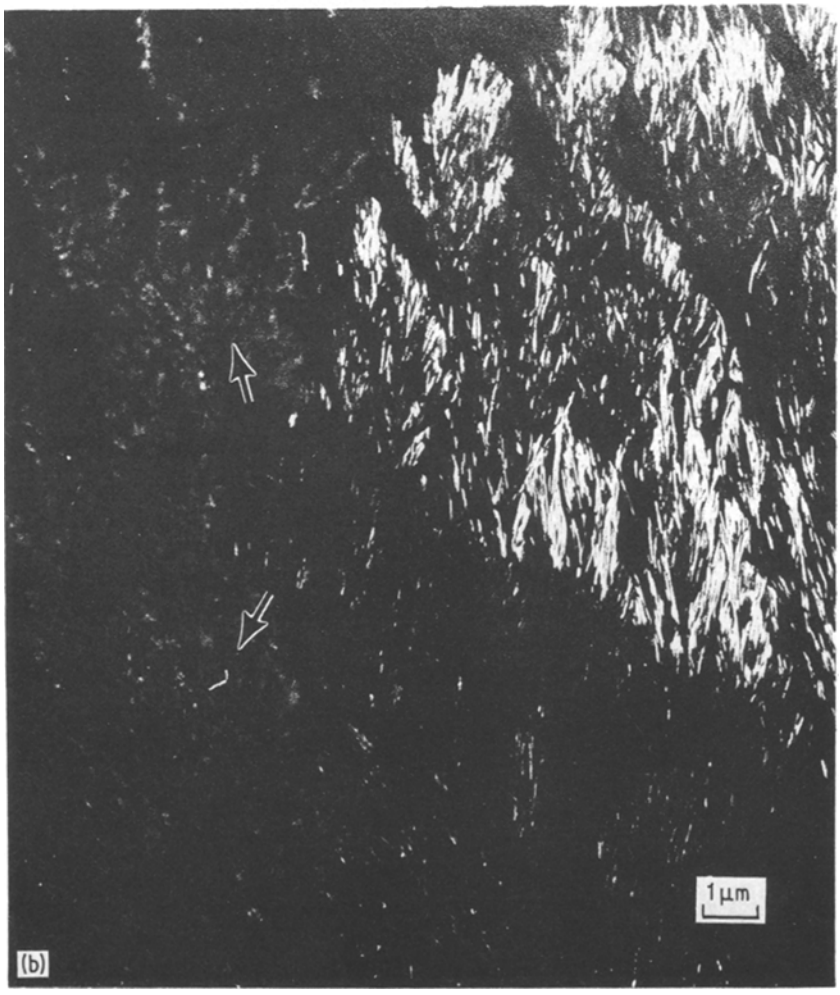

Figure 14 Dark-field diffraction contrast electron micrographs showing the tetragonal crystals in a melt-crystallized PB-L thin film. The micrographs were taken 24 h after the sample had been cooled from the melt. Imaging was done with the tetragonal 200 diffraction. (a) Typical region, (b) region showing irregular grey areas (denoted by arrows) believed to be the image of tetragonal crystals lying almost parallel to the sample surface.

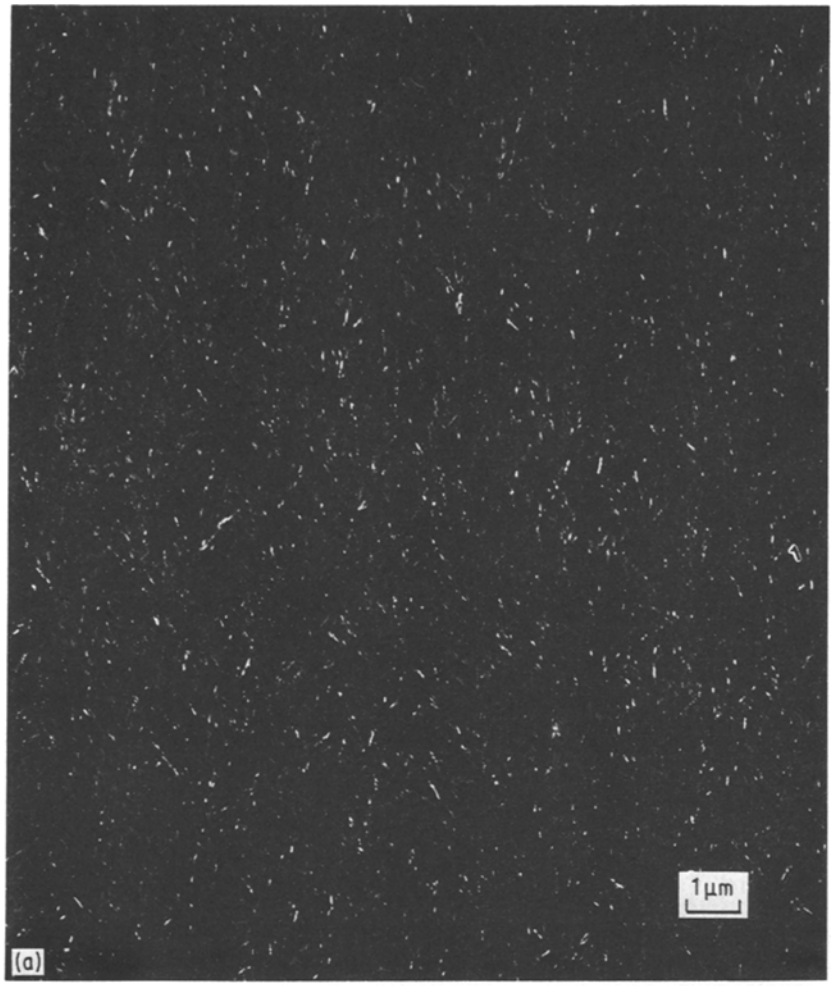

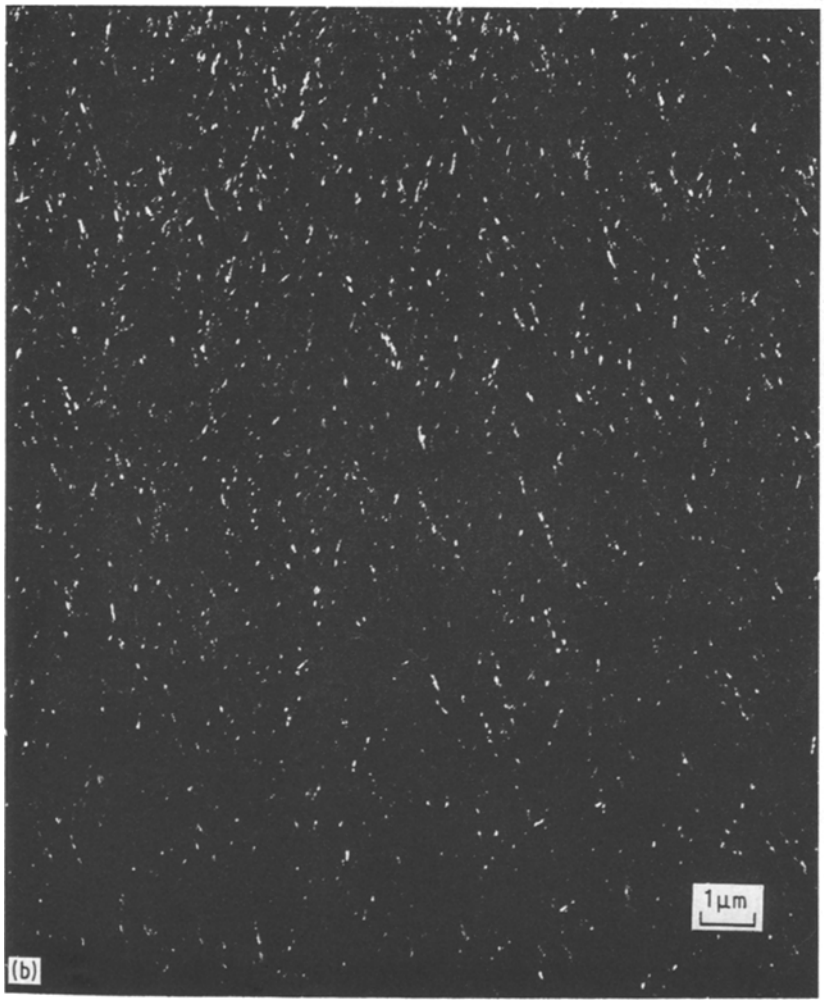

Figure 15 A typical dark-field diffraction contrast electron micrograph showing the twinned hexagonal crystals in melt-crystallized thin films. The micrograph was taken after the sample had been aged at room temperature for 4 months. Imaging was done with the twinned hexagonal 2 2 0 and 3 0 0 diffractions. (a) PB-H, (b) PB-L.

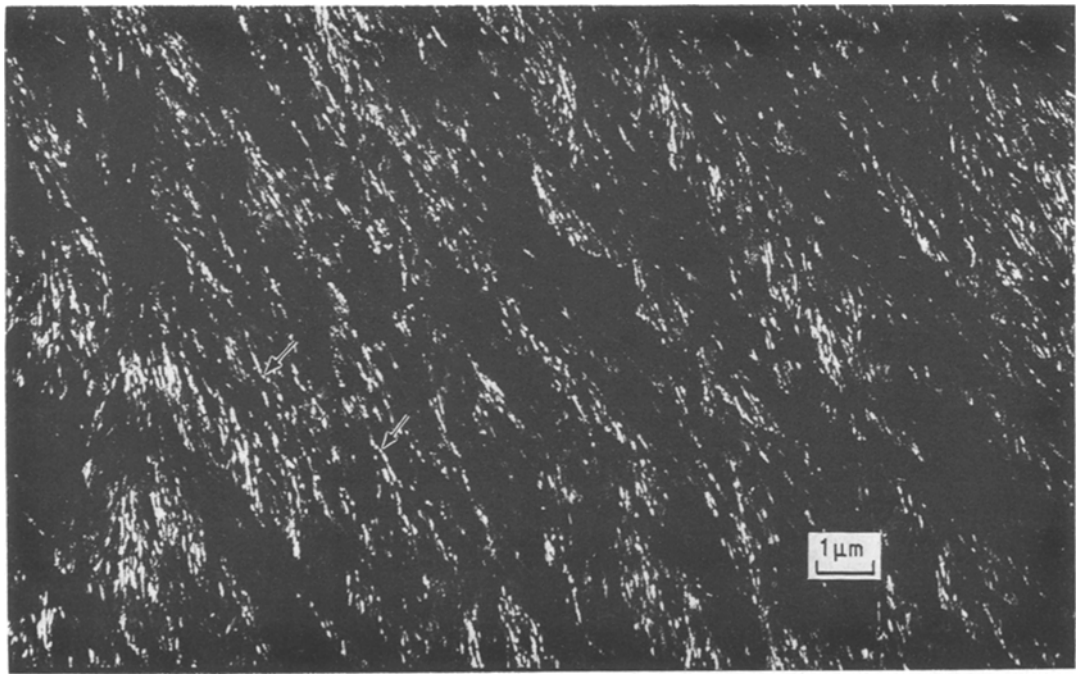

Figure 16 A typical dark-field diffraction contrast electron micrograph of a partially transformed area in a melt-crystallized PB-L thin film. The micrograph was taken after the sample had been aged at room temperature for 10 days. Imaging was done with the tetragonal 2 0 0 and twinned hexagonal 1 1 0 diffractions. The arrows indicate crystallites which lie in rows. Each row of crystallites is believed to have originated from a single tetragonal fibril.

Avrami analysis suggests the initial stage of the transformation is instantaneously nucleated, i.e. at the time of crystallization, the twinned hexagonal "nuclei" are present and begin growth from the beginning. The dark-field micrographs, on the other hand, suggest the "nucleation" is sporadic in time and place. Long tetragonal crystals can be found as long as tetragonal reflections remain in the electron diffraction patterns. It is thought that the initial stage of the transformation is "instantaneously nucleated". The majority of the tetragonal crystals transform in this way. The secondary transformation stage is presumably due to the tetragonal crystals in which the transformation is not "nucleated" at the beginning, either because they themselves form during the room temperature ageing or because the initial nuclei are lacking. This suggests that it is growth of the stable phase that is the rate-determining step in the initial portion of the phase transformation and nucleation in the latter stage.

Solution-grown multilayered tetragonal single crystals transform spontaneously (Figs 17 and 18), in agreement with the previous observation of Holland and Miller [10]. The process is complete in 5 days at room temperature on a carbon substrate. No change in appearance is seen in shadowed samples. A dark-field image of a typical tetragonal crystal is shown in Fig. 17. Moiré lines can be seen on some of the overgrowths suggesting a large crystal (domain) size. A dark-field image of a typical twinned hexagonal crystal obtained on ageing is shown in Fig. 18b. The individual crystal domains appear to be smaller. In agreement with our results from melt-crystallized thin films, this suggests multiple nucleation within each single crystal. Contrary to the results of Holland and Miller [10], however, we find no crystallographic relationship between the tetragonal and resultant twinned hexagonal crystals. They reported [10] that individual sectors of the square tetragonal crystal transformed to only one hexagonal crystal orientation, i.e. twinning did not occur within a sector. The difference may be due to the more complicated, multifold domain nature of the sectors in our crystals.

Our measurements show that the transformation rate is lower in the high molecular weight sample (Table II). Because of the presumably larger coil size and number of entanglements in the melt in the high molecular weight sample, one would expect the solid to contain a higher concentration of taut tie molecules. Hence, contrary to the suggestion of Gohil *et al.* [18], an abundance of taut tie molecules cannot be a predominant factor which determines transformation rate. The fact that multilayered tetragonal single crystals, which contain few or no tie molecules, transform spontaneously leads one to conclude that taut tie molecules are not essential for phase transformation to occur. Rather, since our results suggest primarily immediate nucleation, a modification of Gohil *et al.*'s suggestion appears plausible, i.e. stresses resulting from cooling and crystallization nucleate the twinned hexagonal phase. These stresses will be exerted by all components of the alternating amorphous layers on the crystalline cores. The higher transformation rate of the low molecular weight sample suggests chain ends, as cilia, may play a role. The effect of stress of any kind is emphasized by the care needed to prevent immediate transformation of films during removal of aluminium foil or even flexure of the films. The second stage of transformation may correspond in part to nucleation in crystals on which there is no initial stress.

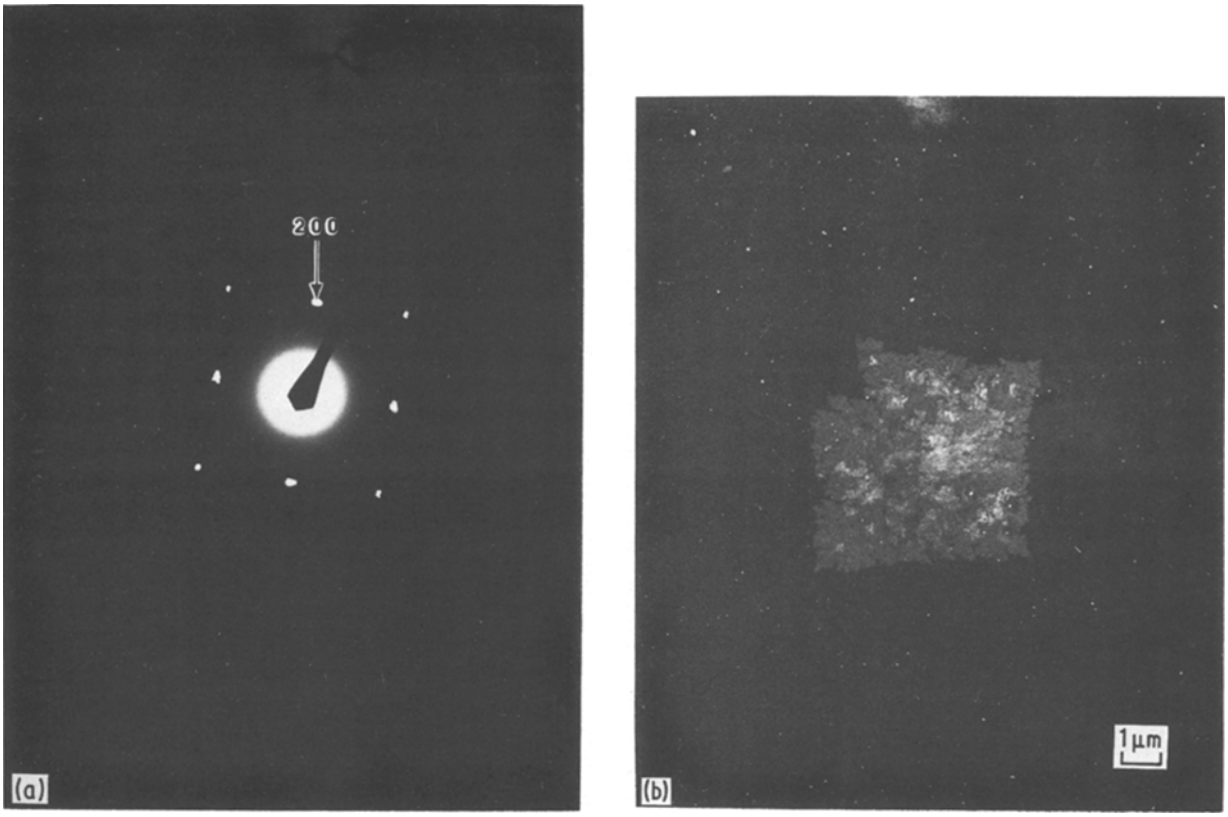

Figure 17 Typical electron diffraction pattern (a) and dark-field diffraction contrast electron micrograph (b) of a typical PB-H tetragonal crystal grown from dilute amyl acetate solution. Imaging was done with one tetragonal 200 diffraction beam.

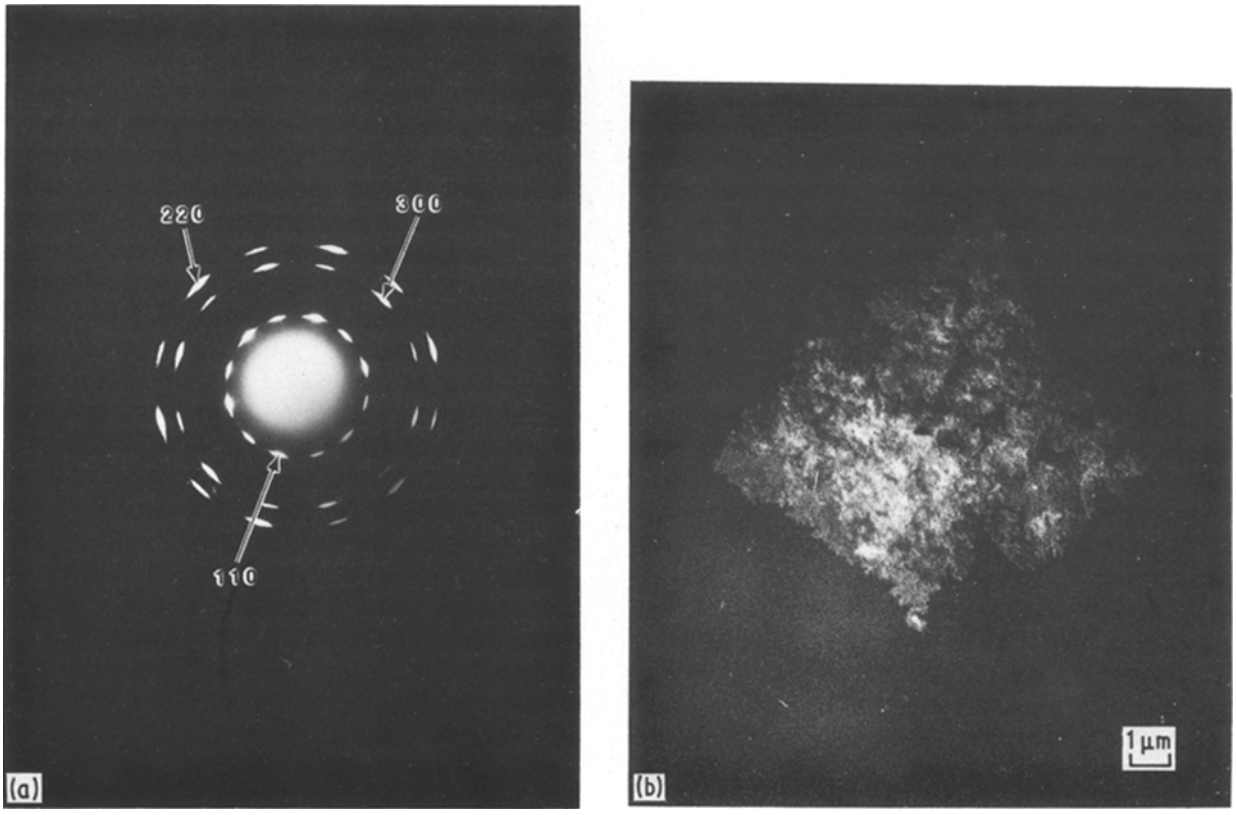

Figure 18 Typical electron diffraction pattern of a twinned hexagonal crystal (a) and dark-field diffraction contrast electron micrograph (b) of a typical twinned hexagonal crystal obtained by ageing its precursor PB-H tetragonal crystal for 1 week at room temperature. Imaging was done with one 220 and one 300 diffracted beam.

4. Conclusions

The main results of this study of the tetragonal → twinned hexagonal crystal phase transformation in PB-1 can be summarized as follows:

1. Nucleation of the stable phase is instantaneous in time. Twinned hexagonal crystal nuclei are believed to form not long after the material has crystallized in the tetragonal form. A slower, second stage of random nucleation is also observed.

2. Growth of the stable phase is the rate-determining step in the initial stage of the transformation.

3. The phase transformation does not affect the surface morphology in either melt-crystallized samples or solution-grown crystals.

4. In the melt-crystallized material, nucleation occurs at random locations throughout a spherulite, rather than as a boundary moving through the spherulite.

5. In both the melt-crystallized samples and our solution-grown crystals, multiple nucleation occurs within a single tetragonal lamella. A number of sets of twinned hexagonal crystals arise from one tetragonal crystal.

Acknowledgements

Appreciation is expressed to the Shell Development Co. for support of this research and to the University of Illinois Materials Research Laboratory and Center for Electron Microscopy for use of their facilities.

References

1. G. NATTA, P. CORRADINI and I. W. BASSI, *Rend. Accad. Naz. Lincei* **19** (1955) 404.
2. G. NATTA, P. PINO, P. CORRADINI, F. DANUSSO, E. MANTICA, G. MAZZANTI and G. MORAGLIO, *J. Amer. Chem. Soc.* **77** (1955) 1708.
3. G. NATTA, P. CORRADINI and I. W. BASSI, *Makromol. Chem.* **21** (1956) 240.
4. G. NATTA, *Experientia Suppl.* **7** (1957) 21.
5. G. NATTA and P. CORRADINI, *Nuovo Cimento Suppl.* **15** (1960) 9.
6. G. NATTA, P. CORRADINI and I. W. BASSI, *ibid.* **15** (1960) 52.
7. G. NATTA, *Makromol. Chem.* **35** (1960) 94.
8. A. TURNER-JONES, *Polym. Lett.* **1** (1963) 455.
9. V. PETRACCONE, B. PIROZZI, A. FRASCI and P. CORRADINI, *Eur. Polym. J.* **12** (1976) 323.
10. V. F. HOLLAND and R. L. MILLER, *J. Appl. Phys.* **35** (1964) 3241.
11. G. GOLDBACH and G. PEITSCHER, *J. Polym. Sci.* **B6** (1968) 783.
12. C. D. ARMENIADES and E. BAER, *J. Macromol. Sci.-Phys.* **B1** (1967) 309.
13. J. BOOR JR and J. C. MITCHELL, *J. Polym. Sci.* **A1** (1963) 59.
14. E. WEYNANT, J. M. HAUDIN and C. G'SELL, *J. Mater. Sci.* **17** (1982) 1017.
15. J. P. LUONGO and R. SALOVEY, *J. Polym. Sci.* **A-2** (1966) 997.
16. T. ASADA, J. SASADA and S. ONOGI, *Polym. J.* **3** (1972) 350.
17. T. ODA, M. MAEDA, S. HIBI and S. WATANABE, *Kobunshi Ronbunshu Eng. Ed.* **3** (1974) 1249.
18. R. M. GOHIL, M. J. MILES and J. PETERMANN, *J. Macromol. Sci.-Phys.* **B21** (1982) 189.
19. B. H. CLAMPITT and R. H. HUGHES, *J. Polym. Sci.* **6** (1964) 43.
20. R. A. AVNER, in "A Basic Statistical Service Package", 11th Edn. (Control Data Corporation, Minneapolis, 1980).
21. M. AVRAMI, *J. Chem. Phys.* **7** (1939) 1103.
22. *Idem, ibid.* **8** (1940) 212.

Received 9 September
and accepted 4 October 1985